Wulff shape of microscopic voids in UO_2 crystals

Martin R. Castell*
Department of Materials, University of Oxford, Parks Road, Oxford OX1 3PH, United Kingdom
(Received 25 February 2003; published 15 December 2003)

UO_2 single crystals with a size of around 1 cm^3 are created in a process involving a period of spectacular grain growth. (111) cleavage cross sections through these crystals expose voids that are typically of μm dimensions. Low voltage scanning electron microscopy of the voids reveals that they are bound by {111} and {001} facets, and some appear to have reached their thermodynamic equilibrium shape (Wulff shape). An analysis of the facet areas shows that the smaller voids are closer to the Wulff shape, and have a surface energy ratio $\varepsilon_{001}/\varepsilon_{111}=1.42\pm0.05$. The larger voids show step bunching at the facet intersections which typically gives rise to ordered step structures of 10s of nm periodicity and produces nanoscale staircases and amphitheatres. Evidence of void ripening by way of connecting channels is also observed.

DOI: 10.1103/PhysRevB.68.235411 PACS number(s): 68.37.Hk, 61.72.Qq, 68.35.Md, 68.47.Gh

I. INTRODUCTION

The rapidly expanding field of surface studies of metal oxides has grown out of their crucial importance in a diverse range of fields in physical sciences.[1] In catalysis they are used either in their pure form or as metal particle supports. Other applications include the change in surface conductivity of certain metal oxides with molecular adsorption which is used in gas sensing. Environmental degradation causing metals to grow a surface oxide is central to work on corrosion studies. The interest in the surface properties of UO_2 stems from the catalytic activity of uranium oxides[2] as well as the effects of surface structure and powder morphology on the sintering behavior of UO_2 used as a fuel in nuclear reactors.

One of the most fundamental properties of surfaces is the energy associated with them. The polar plot of the surface energy versus crystallographic orientation is known as the γ plot, and the thermodynamic equilibrium shape of the crystal (also called the Wulff shape or crystal habit) is determined through the Wulff construction of the γ plot.[3,4] Generally the γ plot has cusps at the low index orientations with the result that the Wulff shape of cubic crystals well below the melting temperature is dominated by low index facets of type {001}, {011}, or {111}. If the surface energies of the different facet types are sufficiently close to each other then more than one facet type will appear in the Wulff shape. In such a case, by measuring the relative areas of the facets on a crystal one can derive their respective surface energy ratios. However, in reality it is very difficult to create an equilibrium crystal. This is due to factors such as the contamination of the surfaces and the interaction with the supporting substrate. There is also the difficulty that the shape of real crystals is inevitably influenced by growth kinetics as well as thermodynamics. Furthermore, the concept of thermodynamic equilibrium is meaningless without stating what the crystal is in equilibrium with.

An approach to circumvent the problems of creating an equilibrium crystal is to investigate empty spaces in crystals that have assumed a thermodynamic equilibrium shape with the gas contained within the space. Empty spaces in crystals have been variously referred to as cavities, pores, voids, bubbles (if filled with gas at high pressure), or holes. Once these empty spaces have reached their equilibrium form, which is generally achieved through extended annealing, the empty spaces are called negative crystals, equilibrium voids, or equilibrium bubbles (if filled with gas at high pressure). In this paper the expressions void and equilibrium void will be used to refer to empty spaces in single UO_2 crystals and their thermodynamic equilibrium structure.

There are a number of previous studies where faceted voids in crystals have been examined. One technique involves using transmission optical microscopy on voids in transparent crystals such as lyotropic liquid crystals,[5] diphenyl crystals,[6] and ice.[7] Transmission electron microscopy of thin foils of equilibrium voids in copper, aluminum, and molybdenum has been used to determine the orientation dependence of the surface energy of those metals.[8] A further technique, also employed in this paper, is to use scanning electron microscopy (SEM) to examine cross sections through voids. This has been done on alumina[9] and quasicrystals,[10] and also demonstrated on UO_2.[11]

Crystals of UO_2 have the face centered cubic fluorite structure. The lowest energy faces are the {111}, {011}, and {001}.[12,13] If the {111} and {001} surface energies are sufficiently close then the crystal habit of UO_2 takes the form of a truncated octahedron, as shown in Fig. 1. The boundary of equilibrium voids within UO_2 will also adopt this shape. The

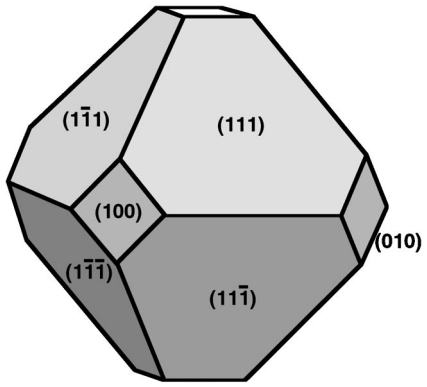

FIG. 1. The truncated octahedron crystal habit or Wulff shape of UO_2. The {111} and {001} faces are indicated. The equilibrium form of a void trapped in a crystal has the same shape.

{001} to {111} area ratio is highly sensitive to the surface energy ratio. Surface energy determination is usually carried out by measuring the contact angle between a liquid metal drop and the surface; however, no studies could be found in the literature where experimental determinations of the surface energies of UO_2 single crystal facets were made. Studies on polycrystalline UO_2 have been carried out,[14] but they are of little relevance to our single crystal studies.

There are some reports of theoretical calculations of UO_2 surface energies. The earliest significant paper on this subject is by Tasker.[15] More recent studies by Abramowski and co-workers[12,13] calculate the surface energies and attachment energies for low index faces using a variety of ionic potentials. Predictions of the equilibrium crystal shape and growth morphology can then be made. They also show how the equilibrium shape is influenced by hydroxilation of the surfaces.

The study presented here is of the examination of microscopic voids in UO_2 crystals that are a relic of the original agglomerate packing arrangement. These residual voids are numerous in quantity and varied in size and shape. By examining (111) cleavage surfaces through UO_2 crystals by low voltage scanning electron microscopy it is possible to show that a significant proportion of the small voids reach their equilibrium shape and are bound exclusively by {111} and {001} facets. The surface areas of the {111} and {001} facets of equilibrium voids are measured, and hence the surface energy ratio of the {001} to {111} surfaces is determined.

II. EXPERIMENTAL PROCEDURES

Cylinders of 11 mm diameter by 13 mm length are pressed from granulated integrated dry route (IDR) UO_2. IDR powder is a strongly agglomerated material of mean particle size 3–4 μm comprising crystallites of size 0.2–0.5 μm. Die wall lubrication is employed during pressing and densities of approximately 6.0 g cm^{-3} result from an applied pressure of about 400 MPa. The porosity in the pressed compact forms two populations comprising the intra-agglomerate porosity of size corresponding to the crystallite size and the inter-agglomerate porosity whose size is related to the agglomerate size.

Pressed pellets are sintered in flowing carbon dioxide in a molybdenum wound alumina tube furnace at a temperature of 1700 °C for 10 h. Early on during the anneal the intra-agglomerate (fine) porosity is annihilated. A conventional grain structure then begins to develop from the agglomerate structure. The interagglomerate porosity is located at triple junctions. Densification up to 99% of theoretical proceeds through additional grain growth (2–3 μm) and continued pore shrinkage until a stage is reached where the grain boundaries break away from pores which then become located within grains. The pores located within grains are then referred to as voids. As sintering proceeds, a conventional microstructure evolves with grain sizes of approximately 20–25 μm. There then follows a period of spectacular grain growth where the grain sizes increase to around 100 μm, following which a few grains grow to several millimetres. The voids are not annihilated during this stage, but persist as a relic of the original agglomerate packing arrangement. A detailed study of the creation of UO_2 single crystals through spectacular grain growth was reported on by Brook and Harrison.[16]

The millimeter grain size pellets are disintegrated into fragmentary single crystals by heating to 2100 °C in flowing dry hydrogen for 1 h in a refractory metal furnace. In addition to pellet disintegration reduction to close to stoichiometry and possibly slightly substoichiometric composition is achieved. Individual millimeter sized single crystals are subsequently selected for analysis.

UO_2 single crystals with dimensions of a few millimeters are fractured in an ambient environment and pieces selected according to the smoothness of the (111) cleavage surfaces. These samples are then mounted onto stubs and transferred into the vacuum chamber of a Hitachi S4500II scanning electron microscope. This microscope is equipped with a cold field emission electron source and is operated using the minimum accessible working distance of 3 mm. The energy of the primary electrons where the observations described in this paper are most clearly seen are 1 keV although higher energies are used on some occasions.

Improvements in low accelerating voltage (0.5–5 kV) performance of high end SEMs mean that spot sizes of 3 nm are routinely achievable at 1 kV. Low voltage imaging has a number of advantages over using the more traditional voltages between 20 and 30 kV, especially when imaging the topography of insulators as shown in this paper. With 1 keV primary electrons the Bethe electron range in UO_2 is 7 nm which is of the order of the escape depth of secondary electrons (SEs). Almost all the detected SEs can therefore contribute to the image contrast, as opposed to the case with high energy primary electrons where a significant proportion of SEs are created from backscattered electrons (BSEs) exiting far from the beam entrance point (called SE2 electrons) which only contribute to the background signal. This factor, combined with the increased stopping power of materials for low energy primary electrons cause the signal to noise ratio to be substantially higher for low keV operation.

The high SE yield at low keV also means that the primary versus SE+BSE currents can balance which allows uncoated insulators to be imaged without suffering from charging artefacts. Overall the increased surface sensitivity and high signal to noise ratio from low voltage operation favors topographic imaging, but this needs to be evaluated against the disadvantages of increased spot size and that contamination is more readily visible.

III. EQUILIBRIUM VOIDS IN UO_2 CRYSTALS

A typical SEM plan view image of a (111) cleavage surface is shown in Fig. 2(a). The lines running across the image are due to steps caused during the cleavage process. The bright symmetrical features are varied in size and density, and are always aligned with their edges parallel to the ⟨110⟩ crystallographic orientations. On first viewing, the symmetrical features appear as if they have a raised topography, but a cleavage section through one of the features reveals that they are in fact voids as shown in Fig. 2(b).

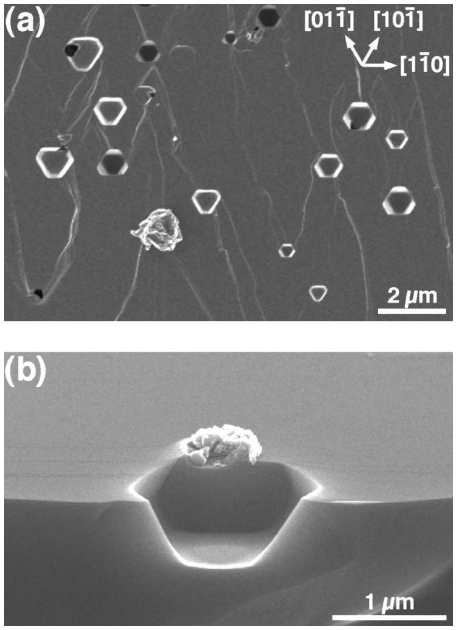

FIG. 2. (a) Secondary electron image (1 keV) of a typical area of a (111) cleavage surface through a UO_2 crystal. The bright symmetrical features of varying sizes have their edges aligned along the ⟨110⟩ crystallographic directions. (b) Oblique angle secondary electron image (20 keV) of a cleavage cross section through one of the symetrical features shows that they are microscopic voids.

When the voids are imaged at high magnification their facetted nature can be seen. Figure 3 shows a series of images of voids of increasing sizes from a void diameter of around 0.5 μm in Fig. 3(a) to a void diameter of around 4 μm in Fig. 3(f). All images are taken with the electron beam perpendicular to the (111) sample surface, and are of voids where the (111) cleavage plane was fortunate enough to traverse the center of the void so that the {001} type facets can be seen. In Fig. 3(d) the facet planes have been indexed to aid image interpretation. The bottom of the void is a (111) facet and can be seen in its entirety. The {111} type facets around it appear substantially foreshortened due to their steep angle with respect to the electron beam. The {001} type facets are also foreshortened, which is why in the image they appear rectangular rather than square. To further aid image interpretation it is helpful to imagine a (111) cross section through the center of the schematic void in Fig. 1, and then view that cross section perpendicular to the (111) plane.

A notable feature of the images in Fig. 3 is the step behavior between the facets. The smallest void shown [Fig. 3(a)] only appears to have {111} and {001} facets, and any other features present are beyond the 3 nm resolving power of the SEM. In Fig. 3(b) some rounding can be seen at the corners where a {001} facet meets two {111} facets. In Figs. 3(c) and 3(d) bunched steps are now evident on the {111} facets near the line where the {111} facets meet. Steps on the {001} facets are also visible. In Figs. 3(e) and 3(f) all {001} facets are surrounded by steps, and {111} facet intersections are also heavily stepped. Generally speaking, the larger voids have a more rounded shape than the small voids and this rounding is associated with bunched steps that can be imaged in the SEM.

One of the aims of this study is to determine the relative surface energies of UO_2 surfaces by measuring the areas of the {111} and {001} facets in equilibrium voids. To achieve that aim one must first select reasonable criteria to decide whether a void is eligible to be classed as having an equilibrium shape. Certainly a necessary criterion is that the void should be symmetrical, i.e., that all {001} faces should be of a similar size and shape. All the voids in Fig. 3 therefore

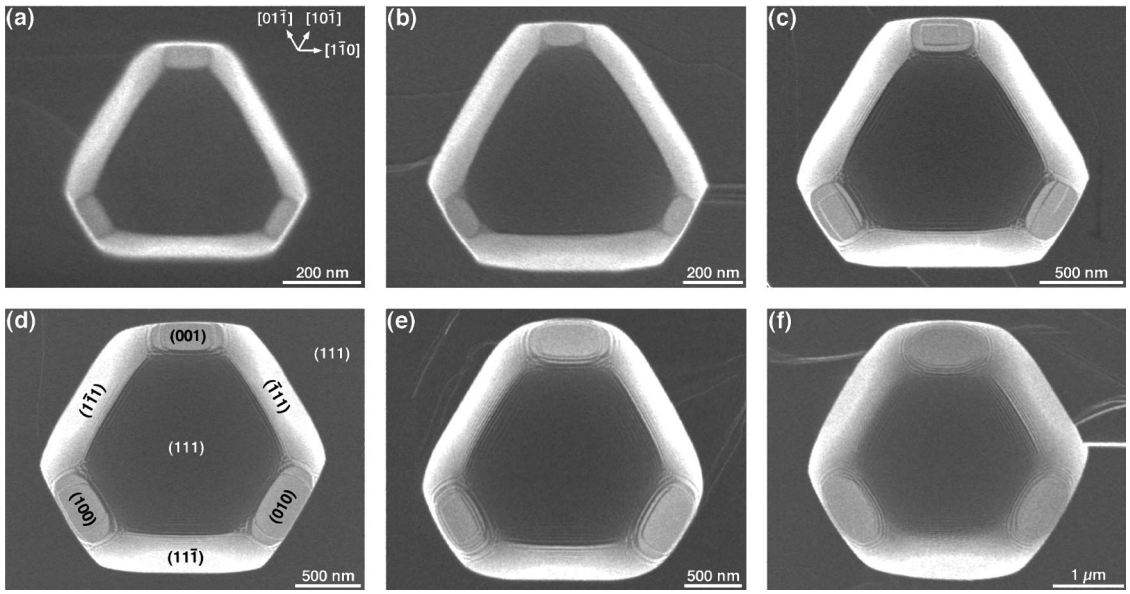

FIG. 3. Secondary electron images (1 keV) of voids of different sizes that are close to the Wulff shape. The crystallographic axes in (a) are applicable to all the images, as are the crystallographic facet assignments in (d). It can be seen that the larger voids (d)–(f) have proportionally more {001} area compared to the smaller voids (a)–(c). Step bunching between the crystal faces is first seen in (c), and becomes more prevalent with increasing void size.

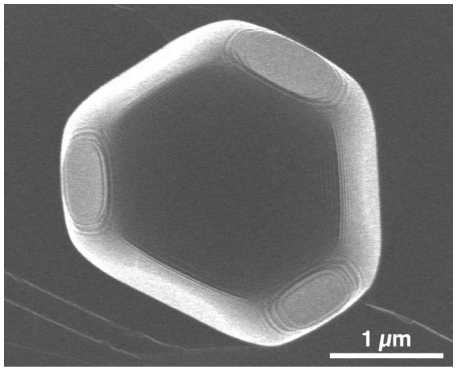

FIG. 4. Secondary electron image (1 keV) of a void with an asymmetric shape.

qualify to have their facet areas measured. An image of a void is shown in Fig. 4, which has an asymmetric shape and must therefore be far from equilibrium. No surface area measurements were carried out on asymmetric voids of the type shown in Fig. 4.

The surface areas of the {111} and {001} facets of symmetrical voids of the type shown in Fig. 3 were determined as follows. A boundary was drawn around the (111) facet that was normal to the electron beam and the area contained within it was measured. This was then taken to be a representative size for all eight {111} facets, so to obtain the total {111} area of the void the measured area was multiplied by a factor of 8. On the same void the horizontal dimensions of the three {001} facets were measured and these dimensions were squared to give the areas of the individual {001} facets. The three {001} areas were added together and multiplied by 2 to reflect that in total there are six {001} faces. This was repeated for 82 images of voids of different sizes. Measurements were only performed on voids that were symmetrical, as described above. The plot of total {001} area to {111} area for 82 voids is shown in Fig. 5(a). This plot presents the data on logarithmic scales and shows the general expected behavior that as the voids increase in size their {111} and {001} facet areas increase proportionately.

Due to the logarithmic nature of the plot in Fig. 5(a) some details are disguised. Figure 5(b) shows the same data, but now plotted as the {001} to {111} facet area ratio against the {111} facet area. In this plot it can be seen that the facet area ratio is relatively constant up to around 5 μm {111} area and thereafter increases significantly. Indeed, simply by looking at the images in Fig. 3 one can see that the larger voids have a relatively larger {001} facet area. The area ratio should clearly remain constant if all the voids are close to thermodynamic equilibrium. How then can the data be interpreted? Another look at Fig. 3 shows that with increasing void size more bunched steps are visible. However, bunched steps should not be a feature of equilibrium voids. The likeliest scenario is therefore that the voids with {111} facet area above 5 μm have not reached the equilibrium shape. The smaller voids are much closer to equilibrium because less mass transport is needed for them to reach that state and they can achieve it more rapidly. This raises the issue of when in the process cycle the voids reach their facetted nature (discussed later).

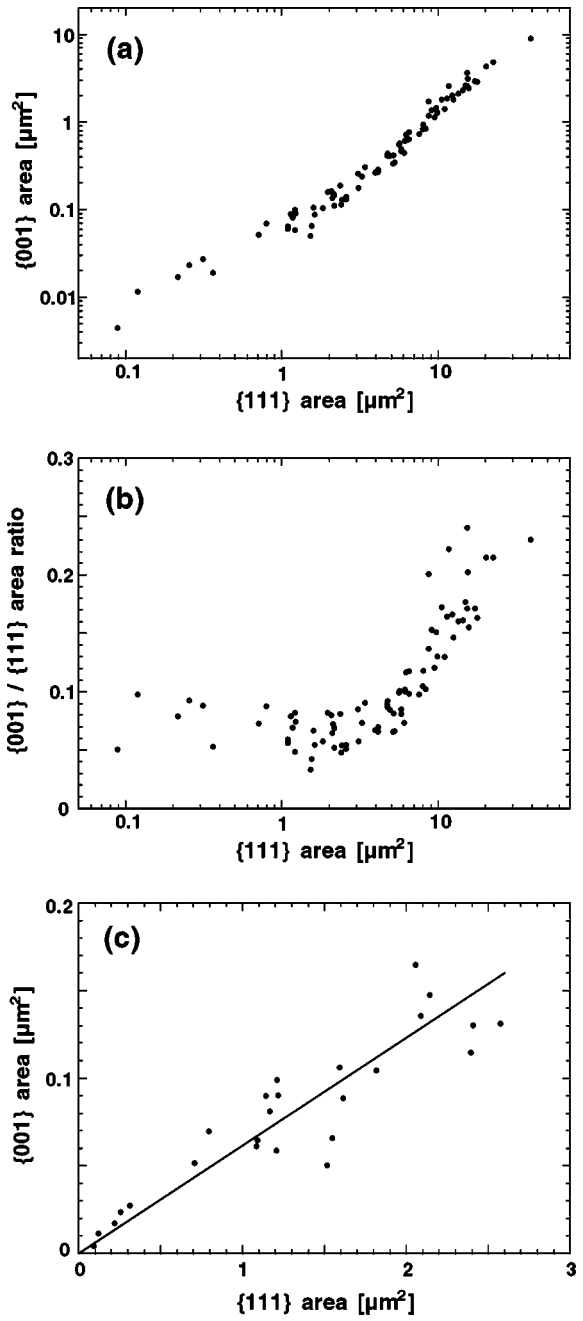

FIG. 5. Statistics of the {001} and {111} surface areas for 82 voids. In (a) the total {001} surface area of a given void is plotted against its total {111} surface area on logarithmic scales. The same data are shown in (b), but plotted as the {001} to {111} area ratio on a linear scale against the {111} area on a logarithmic scale. It can be seen that beyond the 5 μm^2 {111} area there is a strong proportional increase in the size of the {001} faces. In (c) only data from voids without step bunching between the facets is shown. The least squares fit to the points has a gradient of 0.0616 with a standard deviation of 0.0194.

Figure 5(c) shows a linear plot of {001} facet area versus {111} facet area for voids that do not contain stepped facets, i.e., voids that are as near equilibrium as can be judged from the SEM images alone. A least squares fit line through the data constrained to pass through the origin has a gradient of

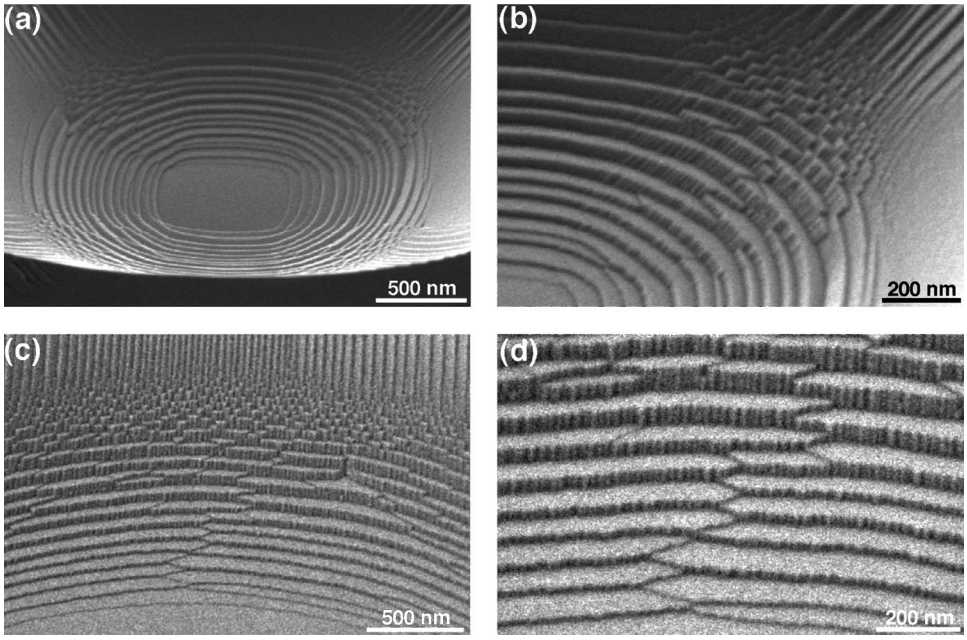

FIG. 6. Secondary electron images (1 keV) of areas in voids where significant step bunching is evident. The micrograph in (a) shows a (001) face in the center of the image with {111} faces leading down to it. Wherever the faces meet there is considerable step formation giving rise to a nanoamphitheater. A magnified view of the top right hand corner of the amphitheater is shown in (b) where the (001) face is at the bottom left of the image and the {111} faces are at the top and right sides of the image. In the region where all three faces meet the step structure becomes highly complex. A similar region to that shown in (b) is shown in (c) except that it is from a much larger void. A staircase of steps rises up and away from the (001) face located at the bottom of the image. A magnified view of the center of (c) is shown in (d), where the rising edges of the steps are seen to be corrugated.

0.0616, with a standard deviation of 0.0194. The ratio

$$\omega = A_{001}/A_{111} = 0.0616 \pm 0.0194$$

will be the value that is used from now on as the measured facet area ratio for equilibrium voids.

A surface energy determination is usually carried out by measuring the contact angle between a liquid metal drop and the surface. Contamination of the surface is clearly a danger with this type of measurement. Another disadvantage is that the accuracy of the surface energy determination is disproportionately affected by errors in the measurement of the contact angle because the measured angle enters into the surface energy versus contact angle equation as a cosine. This means that a typical 1° error in the contact angle will produce a 10% error in the surface energy. In the method used in this paper no absolute values of surface energy can be measured, but the surface energy ratios can be determined with much higher accuracy than by measuring a contact angle. The relationship between the surface area ratio (ω) and the surface energies (ε_{001}, ε_{111}) for the truncated octahedron of the shape shown in Fig. 1 is

$$\frac{\varepsilon_{001}}{\varepsilon_{111}} = \sqrt{3} - \sqrt{\frac{\sqrt{3}\omega}{1+\sqrt{3}\omega}} = 1.42 \pm 0.05.$$

Because the area ratio ω enters the equation under a square root, any measurement errors are reduced accordingly. Measuring surface area ratios can therefore be a very sensitive method for the determination of surface energy ratios.

IV. VOIDS FAR FROM EQUILIBRIUM AND THEIR STEP BEHAVIOUR

In Fig. 4 an image of a void was shown that is far from equilibrium due to the asymmetry of its shape. In Fig. 6 further images from nonequilibrium voids are shown, but now the emphasis is on the step bunching within the voids. Figure 6(a) shows an oblique view of a void with a {001} facet in the center of the image. Surrounding the facet there is extensive step formation. The image is effectively one of an amphitheater where the {001} facet is the field of play and the bunched steps around it form a staircase that is the seating area. A detail of the top right hand corner of Fig. 6(a) is shown in Fig. 6(b), where the complex nature of the steps is particularly evident in the region where the {001} facet meets two {111} facets.

An image of a similar area to that of Fig. 6(b), the corner seating of the amphitheatre, is shown in Fig. 6(c). At the bottom of the image there is a {001} facet which is a flat area that leads into the staircase. Moving away from the {001} facet the steps get higher and narrower until finally at the top of the image the staircase gives way to ridges that are typical of the boundary between two {111} facets. A detailed image of the center of the staircase is shown in Fig. 6(d). The tops of the steps, which appear light in the image, are areas of {001} parallel to the {001} facet. The rising side of the steps are geometrically constrained to be close to the {011} orientation. However, the {011} areas appear to form small ridges with {111} type facets which can be seen in the image as vertical stripes with a separation of around 15 nm. The ob-

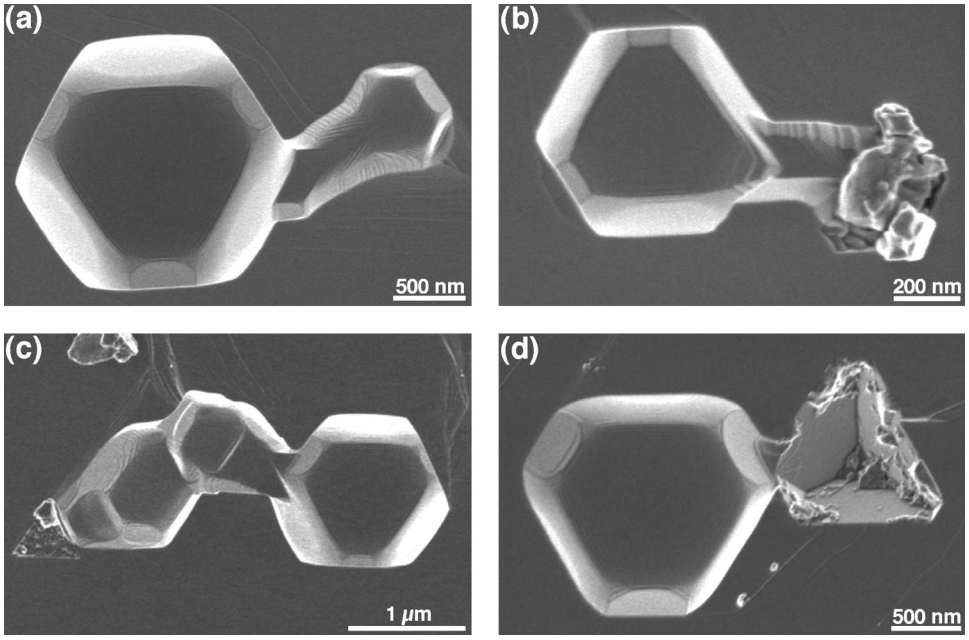

FIG. 7. Secondary electron images (1 keV) of voids that are joined together. In (a) two voids are linked by a channel that aids the vacancy diffusion process. In (b) the right hand void has been filled through accumulation of diffused material from the larger void on the left. The image in (c) shows a group of three voids that are in the process of ripening. In (d) the void on the right is composed entirely of {001} type facets.

servation that a {011} surface transforms into ridges of {111} type is not new, and has been studied by transmission electron microscopy.[17] Theoretical calculations[12] of the {011} surface energy also support the observation that a {011} surface will transform into a surface with ridges that have {111} facets. The additional surface area created by this transformation is more than compensated for by the much lower surface energy of {111} compared to {011}.

A further type of nonequilibrium void are those that are either rapidly growing or shrinking. There will always be a degree of Ostwald ripening that occurs due to vacancy diffusion in the bulk which will affect all voids, but if two voids are joined by a channel then this ripening process will be severely accelerated because surface vacancies in the channel can diffuse much more rapidly than bulk vacancies. Figure 7(a) is an image of a large and a small void that are joined by a channel. In this situation surface vacancies and adatoms can diffuse rapidly between the voids via the connecting channel. The total surface area reduction of this geometry will involve a net diffusion of surface vacancies from the small void to the larger void until there is one remaining large void. In Fig. 7(b) an image of another void pair shows how the ripening process has progressed further. The smaller void to the right has been filled in with diffused material that presumably mainly originated from the larger void on the left. The filled in material in the smaller void looks like it is polycrystalline. Figure 7(c) shows three voids that are joined together. A relic of part of the left hand void can be seen to its left as a triangle with an irregular surface, indicating that there has been some progress towards turning these three voids into one large void. Figure 7(d) shows two voids that are connected together. The left hand void is the usual shape, but the right hand void consists only of {001} facets and has a relatively rough interior possibly indicating growth inside the void. Approximately 10% of the voids observed consist only of {001} facets. They are normally located next to a void of the usual shape, have a rough interior, and are generally less than 1 μm in diameter. Without studying the void shape dynamics *in situ* it is not possible to make definitive statements, but it would appear that the voids dominated by {001} facets are in the process of rapid shrinking, or possibly contain impurities that affect the surface energy balance.

V. DISCUSSION

From the evidence reported in this paper it is possible to make a reasonable proposal concerning the evolution of the void shapes during the process cycle. During the spectacular grain growth at 1700 °C the empty spaces in the single crystals will not initially have any particular shape. However, once the voids are located within single grains, diffusion of vacancies and adatoms on the interior surface of the voids will start to bring them towards their equilibrium shape at that temperature in equilibrium with the gas trapped in the void interior. The subsequent anneal at 2100 °C is sufficiently close to the UO_2 melting temperature of 2840 °C for the voids to become more spherical in shape, because the Wulff shape of the voids depends on temperature. At the melting point voids will be spherical, and as the material is cooled the voids will start to develop facets. At the 2100 °C anneal temperature the Wulff shape of the voids is more spherical than at room temperature. A crucial factor therefore is the rate at which the crystals are cooled from 2100 °C to room temperature. If that cooling rate is so fast that the crystals are effectively quenched then the Wulff shape of the voids at 2100 °C will be retained. However, in the experiments performed here the cooling was simply the rate at which the refractory metal furnace cools after it has been switched off. This gives rise to a peculiar effect. The larger voids require more time than the smaller voids to reach the Wulff shape for any given temperature because more mass transport is required for the larger voids. So what is an adequate cooling rate to maintain the Wulff shape for a small void may be too rapid for a larger void. As the crystals cool

from 2100 °C to room temperature the small voids adjust their shape accordingly, whereas the larger voids cannot do this fast enough. The result is that the small voids can attain a low temperature Wulff shape whereas the larger voids retain more of the higher temperature Wulff shape and contain a lot of steps indicative of their attempts to change shape. To test this proposal further experiments with variable cooling rates need to be performed.

In Sec. III the {001} to {111} surface energy ratio was determined through facet area measurements. How do these relate to the theoretical calculations of the UO_2 surface energy? It should be noted that modeling these surfaces is in itself not without difficulties because strong correlations of the $5f$ electrons complicate the electronic structure of UO_2. *Ab initio* calculations therefore contain a number of problems that have only recently been overcome.[18] For the most up to date surface energy calculations[12,13] of UO_2 only an ionic description of the lattice was used. This work shows that for the preferred interatomic potential and {001} termination the calculated surface energies are 2.72 Jm^{-2} for the {001} surface and 1.27 Jm^{-2} for the {111} surface. This gives a surface energy ratio of 2.14, as compared with the experimentally determined figure reported here of 1.42 ± 0.05. But how reliable are the calculations? Previous experimental studies of the surfaces of UO_2 have shown that the {111} surface is a relaxed bulk termination.[11,19–22] Its atomic structure is well known and the surface energy calculation is therefore presumably reliable. However, the same is not the case for the {001} surface. The polar nature of the {001} surface requires that it reconstruct in order to prevent it from having an infinite surface dipole[15] and there are many conceivable ways for it to do this. Abramowski and co-workers[12,13] investigated the energetics of many different possible reconstructions, but experimental studies show that none of these reflect the highly complex {001} termination observed experimentally.[23] It is therefore quite likely that the surface energy of the {001} face is less than that calculated by Abramowski and co-workers. A reduction of the calculated ε_{001} value would bring the theoretical and experimental results into closer agreement.

From the studies presented here it is assumed that the voids are not filled with gas at any significant pressure. However, gas filling of voids does occur and gives rise to bubbles where in some cases the pressure can be high enough to solidify the gas.[24] If gas at high pressure is contained within the voids of the UO_2 crystals then this would have an impact on the shape of the voids. This issue remains a point for further investigation.

VI. CONCLUSION

The surface energy is a fundamental materials property which affects the macroscopic shape of a crystal. However, surface energy measurements are not routinely carried out due to complications with contamination and measurement errors. These difficulties can be overcome through measurement of facet areas in voids which is shown here to be a highly sensitive way of determining surface energy ratios.

In this paper SEM images are shown of cross sections through faceted voids in UO_2 single crystals. The small voids appear to have reached the equilibrium or Wulff shape. By measuring the facet areas a surface energy ratio of $\varepsilon_{001}/\varepsilon_{111} = 1.42 \pm 0.05$ was determined. The larger nonequilibrium voids often show complex step bunching that is due to growth, shrinking, or shape change of the voids and give rise to nanoscale staircases and amphitheatres.

ACKNOWLEDGMENTS

At the University of Toronto I would like to thank Doug Perovic for provision of SEM facilities, and Fred Neub and Sal Boccia for their assistance with the SEM operation. At Oxford I am very grateful to Andrew Briggs, Christiane Nörenberg, Sergei Dudarev, Adrian Sutton, and John Hunt for stimulating discussions. At BNFL Springfields I would like to thank Dave Goddard and Geoff Wood for their expertise and helpful comments. Funding for this research was provided by the Royal Society and BNFL.

*Email address: martin.castell@materials.ox.ac.uk

[1] V. E. Henrich and P. A. Cox, *The Surface Science of Metal Oxides* (Cambridge University Press, Cambridge, U.K., 1994).
[2] G. J. Hutchins, C. S. Heneghan, I. D. Hudson, and S. H. Taylor, Nature (London) **384**, 341 (1996).
[3] M. C. Desjonqueres and D. Spanjaard, *Concepts in Surface Physics* (Springer, Berlin, 1996).
[4] G. Wulff, Z. Kristallogr. **34**, 449 (1901).
[5] P. Sotta, J. Phys. II **1**, 763 (1991).
[6] A. Pavlovska and D. Nenow, J. Cryst. Growth **8**, 209 (1971).
[7] Y. Furukawa and S. Kohata, J. Cryst. Growth **129**, 571 (1993).
[8] R. S. Nelson, D. J. Mazey, and R. S. Barnes, Philos. Mag. **11**, 91 (1965).
[9] M. Kitayama and A. M. Glaeser, J. Am. Ceram. Soc. **85**, 611 (2002).
[10] F. Kluge, M. Yurechko, K. Urban, and P. Ebert, Surf. Sci. **519**, 33 (2002).
[11] M. R. Castell, S. L. Dudarev, C. Muggelberg, A. P. Sutton, G. A. D. Briggs, and D. T. Goddard, Microsc. Microanal. **6**, 324 (2000).
[12] M. Abramowski, R. W. Grimes, and S. Owens, J. Nucl. Mater. **275**, 12 (1999).
[13] M. Abramowski, S. E. Redfern, R. W. Grimes, and S. Owens, Surf. Sci. **490**, 415 (2001).
[14] R. O. A. Hall, M. J. Mortimer, and D. A. Mortimer, J. Less-Common Met. **121**, 341 (1986).
[15] P. W. Tasker, Surf. Sci. **78**, 315 (1979).
[16] R. J. Brook and K. T. Harrison, *The Achievement of Spectacular Grain Growth in UO_2 Fuel* (UKAEA Harwell, 1975).
[17] V. Krasevec and B. Navinsek, Phys. Status Solidi A **30**, 501 (1975).
[18] S. L. Dudarev, D. N. Manh, and A. P. Sutton, Philos. Mag. B **75**, 613 (1997).
[19] M. R. Castell, C. Muggelberg, G. A. D. Briggs, and D. T. Goddard, J. Vac. Sci. Technol. B **14**, 966 (1996).
[20] C. Muggelberg, M. R. Castell, G. A. D. Briggs, and D. T. God-

dard, Surf. Rev. Lett. **5**, 315 (1998).
[21] M. R. Castell, C. Muggelberg, S. L. Dudarev, A. P. Sutton, G. A. D. Briggs, and D. T. Goddard, Appl. Phys. A: Mater. Sci. Process. **66**, S963 (1998).
[22] M. R. Castell, S. L. Dudarev, C. Muggelberg, A. P. Sutton, G. A. D. Briggs, and D. T. Goddard, J. Vac. Sci. Technol. A **16**, 1055 (1998).
[23] C. Muggelberg, M. R. Castell, G. A. D. Briggs, and D. T. Goddard, Appl. Surf. Sci. **142**, 124 (1999).
[24] P. J. Goodhew, Mater. Sci. Technol. **6**, 950 (1990).